Energy, Environmental, and Catalysis Applications

Improving the Stability and Efficiency of CuO Photocathodes for Solar Hydrogen Production through Modification with Iron

Ainhoa Cots, Pedro Bonete, and Roberto Gómez

ACS Appl. Mater. Interfaces, **Just Accepted Manuscript** • DOI: 10.1021/acsami.8b09892 • Publication Date (Web): 17 Jul 2018

Improving the Stability and Efficiency of CuO Photocathodes for Solar Hydrogen Production through Modification with Iron

*Ainhoa Cots, Pedro Bonete, Roberto Gómez**

Departament de Química Física i Institut Universitari d'Electroquímica, Universitat d'Alacant, Apartat 99, E-03080 Alacant, Spain

KEYWORDS cupric oxide, photocathode, stability, water splitting, iron oxide, overlayer

ABSTRACT

Cupric oxide (CuO) is considered as a promising photocathode material for photo(electro)chemical water splitting due to its suitable band gap, low cost related to copper earth abundancy and straightforward fabrication. The main challenge for the development of practical CuO-based photocathodes for solar hydrogen evolution is to enhance its stability against photocorrosion. In this work, stable and efficient CuO photocathodes have been developed by using a simple and cost-effective methodology. CuO films, composed of nanowires and prepared by chemical oxidation of electrodeposited Cu, develop relatively high photocurrents in 1 M NaOH. However, this photocurrent appears to be partly associated to photocorrosion of CuO. It is significant though that, even unprotected, a Faradaic efficiency for

hydrogen evolution of ~45% is attained. The incorporation of iron through an impregnation method, followed by a high-temperature thermal treatment for promoting the external phase transition of the nanowires from CuO to ternary copper iron oxide, was found to provide an improved stability at the expense of photocurrent, which decreases to about one third of its initial value. In contrast, a Faradaic efficiency for hydrogen evolution of ~100% is achieved even in the absence of co-catalysts, which is ascribable to the favorable band positions of CuO and the iron copper ternary oxide in the core shell structure of the nanowires.

INTRODUCTION

In the last decades, the consumption of fossil fuels has increased rapidly due to the increase of the global energy demand, thus raising environmental concerns, such as that associated with the emissions of pollutant gases, *i.e.* greenhouse gases. Considering this and the depletion of oil reserves, it seems necessary to investigate environmentally friendly alternative sources of energy. In this context, semiconductor oxides constitute a class of materials extensively studied for the development of next-generation energy conversion and storage devices. Specifically, they are being employed as electrodes in a number of electrochemical devices, such as dye-sensitized solar cells,[1-3] sodium-ion batteries,[4-5] supercapacitors,[6] and photoelectrochemical cells,[7] among others.

It is now widely accepted that sustainability requires to find an efficient strategy to convert and store solar energy into chemical fuels, such as hydrogen. Artificial photosynthesis has been re-gaining great attention as a way to obtain carbon-free clean energy.[8,9] Photoelectrochemical (PEC) devices appear to constitute a promising option for generating and storing chemical fuels

such as hydrogen gas, a carbon-free fuel with high energy density, in a clean and renewable way, since they can achieve the direct conversion of solar energy into chemical fuels.[10–12]

The minimum energy necessary to overcome the thermodynamic and kinetic barriers for water splitting is about 2 eV. However, a single semiconductor material capable of leading to a high solar-to-hydrogen (STH) conversion efficiency has not been found yet.[13,14] On the other hand, the conversion efficiency can be improved by means of tandem cells comprising a photocathode where solar hydrogen evolution takes place and a photoanode where water oxidation occurs.[15–17] In addition, employing two photoelectrodes in tandem presents several advantages compared to the use of photovoltaic devices in tandem with photoelectrodes, highlighting the approach of the semiconductor-liquid junctions in order to separate the photogenerated carriers. Specifically, this configuration minimizes the complexity and the potential cost of the device.[15,16,18,19] The selection of semiconductors with small band gap and complementary light absorption is critical for obtaining efficient water splitting devices.[10,20–22]

There are still some barriers for the application of semiconductor materials as practical photoelectrodes: *(i)* absorption spectra should match the solar spectrum as to increase the solar energy conversion; *(ii)* materials must be stable in aqueous electrolytes under illumination to ensure long lifetime; *(iii)* materials should be based on earth-abundant elements to allow the highest performance/cost ratio possible.[23] Focusing on these challenges, the employment of metal oxides seems to be one of the best options due to their typically simple synthetic procedure, and high stability compared to other compounds.

In addition, the materials employed as photocathodes should fulfil another condition, namely, the potential of its conducting band edge should be significantly more negative than the H_2O/H_2

potential as to overcome the hydrogen evolution overpotential. Keeping this in mind, only a limited number of oxides can potentially be employed as photocathodes. In recent years, some p-type metal oxides have been studied in this context including binary oxides such as CuO (1.3-1.7 eV)[22,24–29] and Cu_2O (2.1 eV),[30–35] and ternary oxides such as $CaFe_2O_4$ (1.9 eV),[36–38] $CuNb_3O_8$ (1.5 eV),[39] $CuFeO_2$ (1.5 eV),[40] $CuCrO_2$ (3.1 eV),[41] and $LaFeO_3$ (2.0 eV).[17,42] Among them, copper (II) oxide seems to be one of the most promising candidates as it could, upon appropriate modification, meet the main requirements mentioned above. Although cupric oxide has not been as widely studied for PEC applications as cuprous oxide, its use as photocathode for hydrogen evolution has been reported in several works.[25,27-29,43-45] In any case, nowadays there is still controversy about the fraction of photocurrent resulting in hydrogen generation or coming from CuO photocorrosion. It seems necessary to protect cupric oxide for making practical its use as a water splitting photocathode. Tilley *et al.* reported TiO_2 atomic layer deposition (ALD) as a protective strategy to stabilize the CuO photocathode, reporting a Faradaic efficiency ~100%.[27] However, using ALD is not particularly appropriate for scale-up production and it would significantly increase the production cost of the photoelectrodes. It seems thus critical to look for new simple and low-cost strategies for protecting CuO electrodes against photocorrosion.

The main objective of this work is to develop and optimize a new low-cost procedure based on surface phase transformation able to protect cupric oxide, hindering its photocorrosion. To minimize the electrode fabrication costs, the synthesis of CuO nanowires consists on a simple electrodeposition-thermal treatment approach. We demonstrate that the addition of iron by a simple and low-cost methodology followed by a thermal treatment, which facilitates the external conversion of the CuO nanowires into a ternary copper iron oxide, can diminish the corrosion of

the CuO photocathodes. We also confirm Faradaic efficiencies close to 100% in the production of H_2 after iron modification.

EXPERIMENTAL SECTION

Synthesis of cupric oxide nanowires. The methodology employed to synthesize cupric oxide nanowires relies on copper metal electrodeposition according to the work by Kang *et al.*[29] followed by a chemical oxidation as proposed by Lin *et al.*[46] and a thermal treatment. All solutions were prepared using deionized water (resistivity ≥ 15 MΩ·cm). The Cu films were electrodeposited at -0.3 V *vs*. Ag/AgCl/KCl_{sat} for 1 h from an aqueous solution containing 0.1 M $Cu(NO_3)_2 \cdot 3H_2O$ (Labkem, Analytical Grade ACS), and 3 M lactic acid (Sigma-Aldrich, 85%) adjusted at a pH of 5 by adding NaOH pellets (Panreac, 98%). The Cu films were chemically oxidized by immersion in a solution containing 2.5 M NaOH (Panreac, 98%) and 0.125 M $(NH_4)_2S_2O_8$ (Sigma-Aldrich, 98%). After 5 min the films were removed from solution, rinsed with water and ethanol, and dried at room temperature. Upon the chemical oxidation process, $Cu(OH)_2$ nanowires were already formed.[46] Finally, the samples were thermally treated at 450 ºC for 1 h in a conventional oven in air, obtaining CuO nanowires.

Protection by employing iron chloride as precursor. The protection of cupric oxide was achieved by employing a simple impregnation method (drop-casting). The precursor used was iron chloride ($FeCl_3 \cdot 6H_2O$, Sigma-Aldrich, 99%). By varying the concentration of the precursor, the thickness of the conversion coating can be controlled. The precursor concentration, the expected coating thickness, and the nomenclature employed for each set of conditions are gathered in Table 1. Immediately after applying the drop-casting procedure, the electrodes were thermally treated in air at 550 ºC to form the ternary copper iron oxide (CIO) shell. Different

conditions were tested for optimizing this procedure. On the one hand, two procedures of precursor application were tested: *(i)* applying the total amount of iron in one droplet and *(ii)* diluting by a factor 1:*n* the precursor solution, and then adding *n* droplets of this solution and drying at 90 ºC between successive additions. On the other hand, for each precursor application mode, two thermal treatment times were tested: *(i)* 10 h and *(ii)* 5 h.

Table 1. Molar concentration of the iron precursor and the depth of CIO in nanometers together with the nomenclature employed. CIO stands for copper iron oxide with the general stoichiometry $CuFe_2O_4$. The volume of a droplet is of 30 µL.

Nomenclature employed	[$FeCl_3$] / mM	Thickness / nm
CIO_1	0.13	3
CIO_2	0.22	5
CIO_3	0.35	8
CIO_4	0.44	10

Sample characterization. The morphology of the different samples was studied by means of FE-SEM micrographs (field emission scanning electron microscopy, Zeis Merlin VP Compact). The microscope employed is equipped with an energy dispersive X-ray spectrometer (EDS, Bruker Quantax 400). The crystal structure of cupric oxide was identified by X-ray diffraction (Bruker D8-Advance, using Cu Kα radiation) with the rotatory anode operating at 40 kV and 40 mA in the 2θ range from 30º to 80º using 0.5 º·min^{-1} as step scan. Raman spectra were obtained with a laser Raman spectrometer (Jasco, NRS-5100), using an excitation line provided by an Ar laser at 531.92 nm. Finally, X-ray photoelectron spectroscopy (XPS) was employed for compositional analysis and for characterization of the copper and iron oxidation states (K-Alpha Thermo-Scientific).

(Photo)electrochemical characterization. A standard three-electrode cell was employed to carry out the (photo)electrochemical measurements, using a cupric oxide film (either pristine or modified with iron) as a working electrode (1.2 cm^2 geometric area) and an $Ag/AgCl/KCl_{sat}$ electrode as a reference electrode (to which all the potentials are referred). A platinum wire was used as a counter-electrode. The electrolyte solution employed was an N_2-purged 1 M NaOH (Panreac, 98%). A scanning potentiostat (Potentiostat/Galvanostat AUTOLAB PGSTAT30) was employed to record voltammograms both in the dark and under illumination at a scan rate of 50 $mV \cdot s^{-1}$ in the case of cyclic voltammetry or 10 $mV \cdot s^{-1}$ in the case of linear voltammetry. Stability tests were made by means of chronoamperometry at a constant potential of -0.4 V under illumination. The experiments were carried out in the following order: first, a linear voltammetry under illumination is recorded and then a cyclic voltammogram in the dark. Electrochemical impedance spectroscopy (range from 10 kHz to 0.1 Hz) was also measured with this instrument. The lamp employed for illumination was a 1000 W ozone-free xenon arc lamp (ORIEL Newport 66921 Lamp power 450-1000 W). The radiation was passed through a water filter and a radiation cut off filter (Newport FSR-KG3 $\lambda \geq 350$ nm). The light intensity was measured with a thermopile (Thorlabs PM100D) with an incident power density of around 320 $mW \cdot cm^{-2}$. Hydrogen gas obtained in a two-compartment glass cell was measured with a Hewlett Packard gas chromatograph (see Supporting Information).

RESULTS AND DISCUSSION

Cupric oxide

Sample characterization. Figure 1 shows the FE-SEM top-view images at different magnifications as well as a cross-section of a cupric oxide thin film. The morphology obtained

corresponds to nanowires with an average diameter of about 70 nm (see the corresponding histogram as an inset in Figure 1a). Figure 1b provides evidence that these nanowires are formed by smaller, more isotropic grains and they are thus polycrystalline. This was checked by means of TEM images (see Supporting Information, Figure S1), which show that the grains tend to be elongated with a length of around 100 nm. As shown in Figure 1a, the films present a rather open structure, allowing for an extended contact with the electrolyte. The cross-section of the cupric oxide nanowire electrode shows a thickness approximately equal to 4 μm (Figure 1c). Importantly, the nanowires are mainly perpendicular to the substrate, which is convenient for minimizing the distance that photogenerated holes need to travel to reach the substrate.

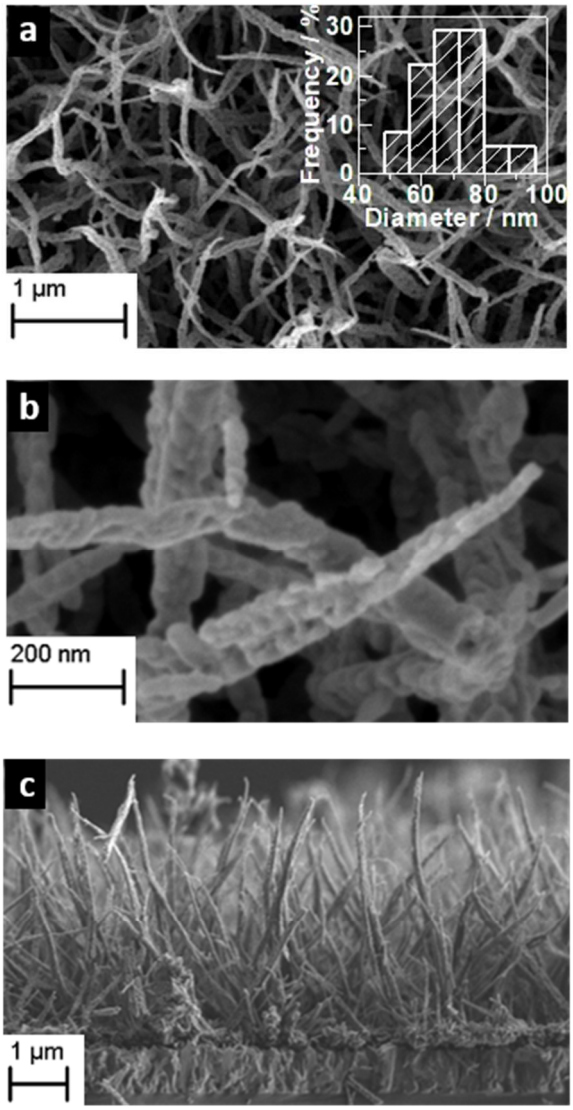

Figure 1. FE-SEM images obtained for pristine cupric oxide, (a, b) top views and (c) cross section. The inset shows the histogram corresponding to the nanowire diameter distribution.

X-ray diffraction (XRD) patterns for cupric oxide films are shown in Figure 2a. The peaks observed were identified using the JCPDS catalog as a reference for standard values. The diffractogram confirms the existence of cupric oxide with monoclinic structure. The unlabeled peaks correspond to SnO_2 (casiterite phase) from the conducting glass substrate. Additionally, the XPS spectra for the Cu 2p region was also monitored (Figure 2b), and it was clearly

established that it corresponds to CuO due to the presence of four 2p peaks. The Cu 2p peaks at 933.7 eV and 953.6 eV correspond to Cu $2p_{3/2}$ and Cu $2p_{1/2}$, respectively, and reveal an oxidation state of +2. The presence of the two shake-up satellite peaks at 942.5 eV and 962.3 eV also indicates the existence of CuO.[46–48]

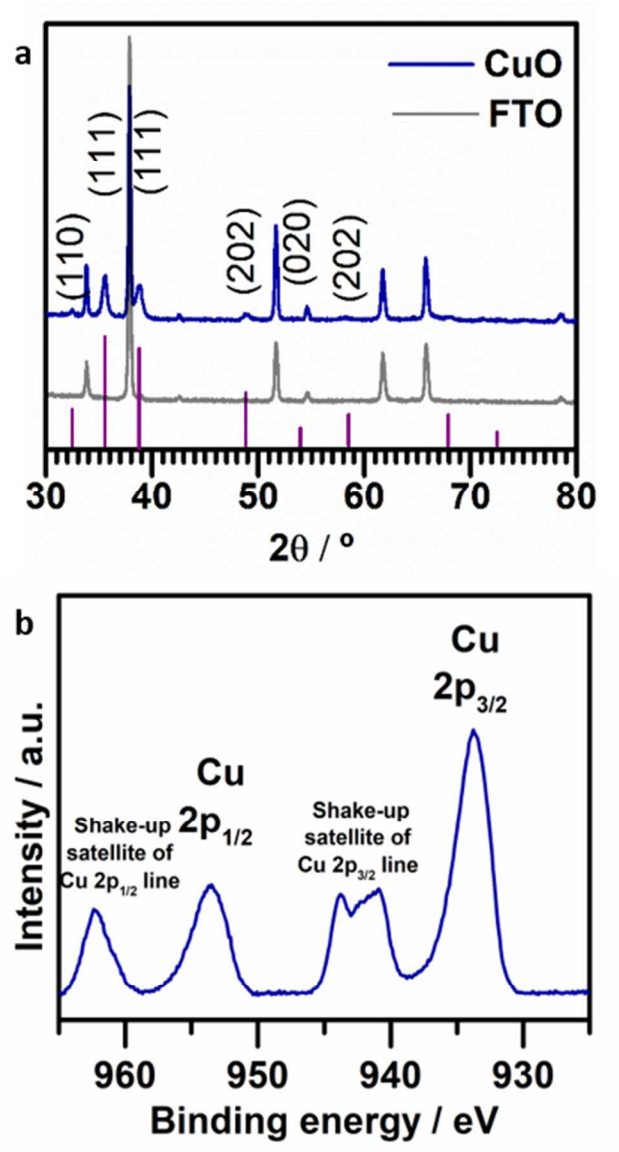

Figure 2. (a) X-ray diffractogram for pristine cupric oxide (blue). The cupric oxide main reflections are labeled. The unlabeled peaks correspond to the conducting glass substrate (F:SnO_2). (b) Cu 2p XPS spectra for pristine copper oxide (II).

(Photo)electrochemical characterization. Figure 3 shows the (photo)electrochemical characterization of pristine copper (II) oxide. Specifically, Figure 3a shows linear scan voltammograms (LSVs) obtained in N_2-purged aqueous 1 M NaOH under both chopped and continuous illumination (320 $mW \cdot cm^{-2}$, $\lambda > 350$ nm). The response of the cupric oxide nanowires has a (photo)onset at about 0.1 V (see supporting information, Figure S3) and the current density increases rapidly upon scanning to more negative potentials, attaining a photocurrent of -1.4 $mA \cdot cm^{-2}$ at -0.4 V. Subsequently, a second LSV was obtained under continuous illumination, showing slightly smaller photocurrents (see dashed line in Fig. 3b), which suggests that cupric oxide is not fully stable under the conditions of the experiment. Immediately after recording the response under illumination, cyclic voltammograms (CVs) not revealing the appearance of significant capacitive currents were obtained in the dark as shown in Figure 3b. While cathodic currents are not recorded in the potential window being investigated, significant oxidation currents appear for potentials above -0.2 V. These are likely due to the re-oxidation of the products associated with the appearance of the cathodic photocurrents (Cu(I) to Cu(II)). Finally, Figure 3c shows a chronoamperogram obtained at -0.4 V for 1000 s under continuous illumination. The photocurrent decreases rapidly, attaining values close to zero after 200 s of continuous illumination due to a severe photocorrosion of the material, indicating that the photocurrents shown in Figure 3a cannot be attributed solely to hydrogen generation.

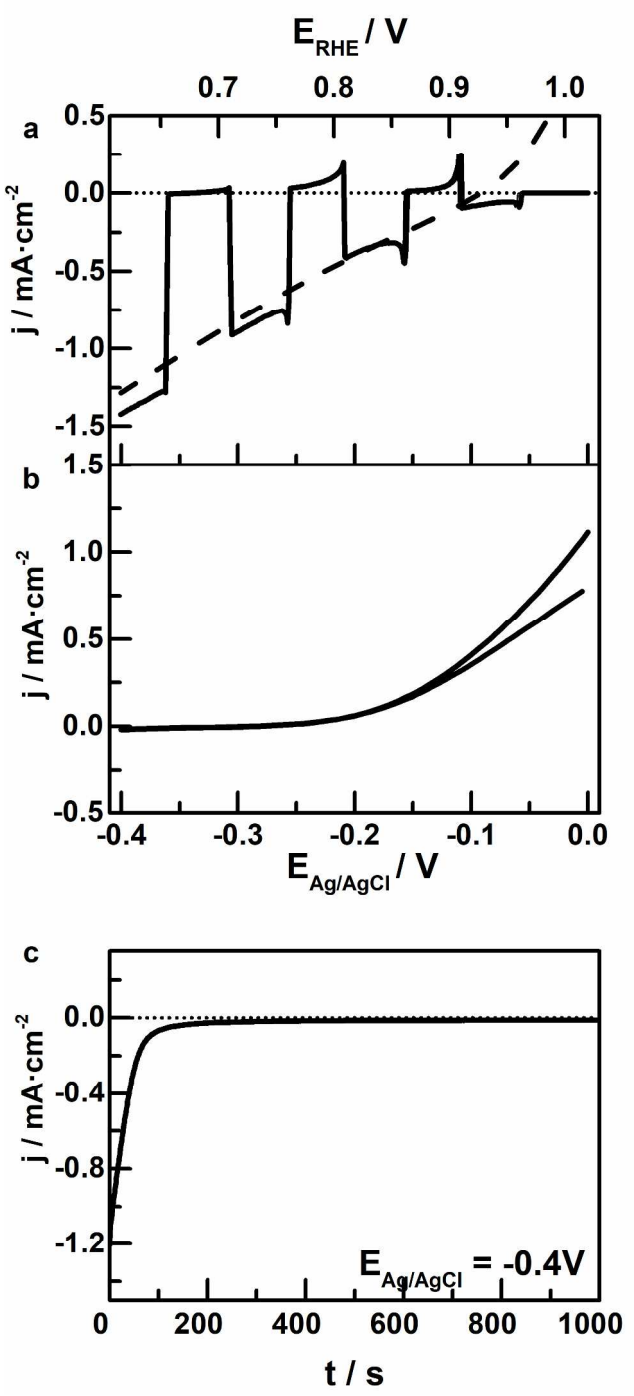

Figure 3. (Photo)electrochemical characterization in N_2-purged aqueous 1 M NaOH for pristine cupric oxide. (a) Linear voltammograms obtained under either chopped (320 mW·cm^{-2}, $\lambda > 350$ nm) or continuous illumination (dashed line), (b) cyclic voltammogram obtained in the dark, and (c) chronoamperometric curve obtained under illumination (320 mW·cm^{-2}, $\lambda > 350$ nm) at an applied potential of -0.4 V *vs.* Ag/AgCl.

Electrochemical impedance spectroscopy (EIS) experiments (Figure 4) were performed under continuous illumination for pristine cupric oxide at two different potentials (-0.10 V and -0.23 V) to characterize the kinetics of the charge transfer processes under PEC operating conditions. Considering that the radius of the semicircle obtained in the high frequency range is associated with the charge transfer resistance (R_{ct}) at the semiconductor/electrolyte interface, at a potential of -0.1 V, R_{ct} would have an approximate value of 0.05 kΩ while at a more negative potential (-0.23 V) R_{ct} diminishes, attaining a value of about 0.03 kΩ. This is the expected behavior for a photocathode and it is compatible with the results shown in Figure 3a.

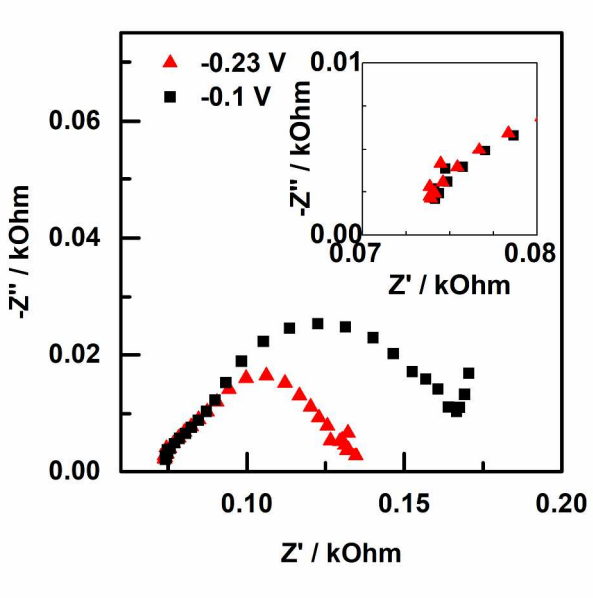

Figure 4. Nyquist plots for pristine cupric oxide at -0.1 V vs. Ag/AgCl (square, black) and -0.23 V *vs.* Ag/AgCl (triangle, red) under illumination (320 mW·cm^{-2}, λ > 350 nm) in N_2-purged aqueous 1 M NaOH.

Cupric oxide modified with iron (CIO)

Sample characterization. Analogously to pristine cupric oxide, copper oxide modified with iron (CIO) was characterized morphologically as shown in Figure 5. Both the FE-SEM top-view images obtained at two different magnifications (Figure 5a and 5b) and the cross-section (Figure 5c) for the electrode CIO_3 are shown. Qualitatively, modification with iron keeps the

morphology of the nanowires unaltered with respect to the case of pristine cupric oxide. However, the average diameter slightly increases from 70 to 88 nm. Corresponding TEM images are shown in Figure S2, although no apparent changes are observed upon modification, probably because of resolution limitations of our instrument. As shown in Figure 5c, the thickness of the film remains unaltered after the incorporation of iron, supporting the notion that the iron added was incorporated as a conformal shell to the nanowires.

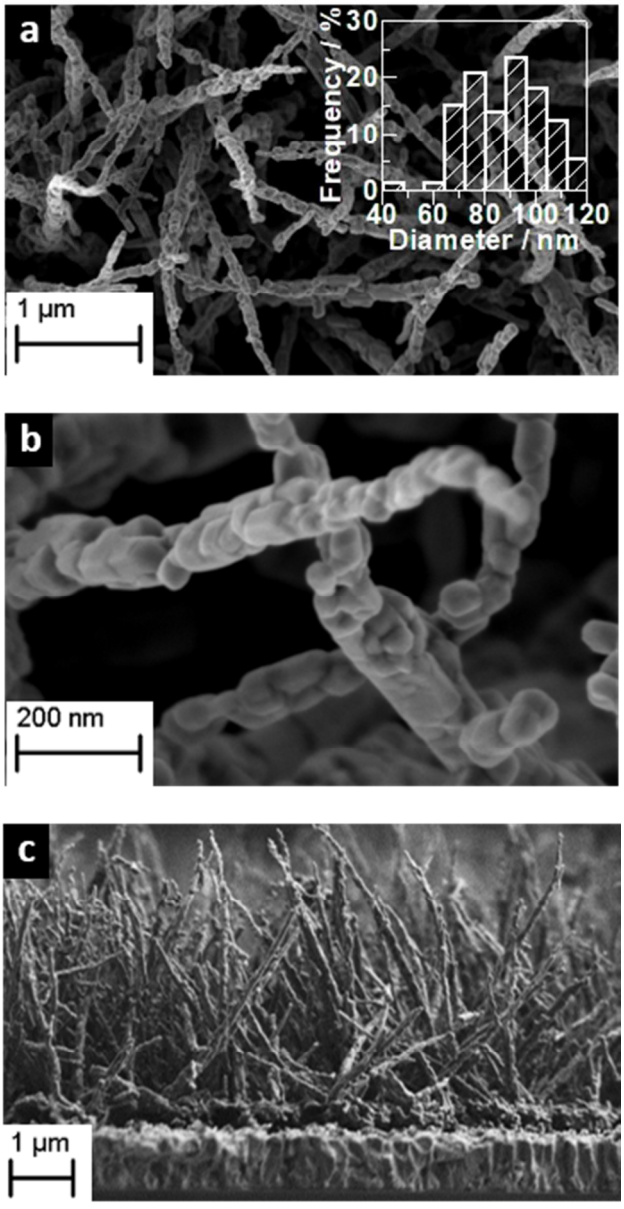

Figure 5. FE-SEM images obtained for an electrode of copper oxide modified with iron (electrode CIO_3), (a, b) top views and (c) cross section. The inset in (a) shows the histogram corresponding to the diameter distribution.

An XRD pattern for the CuO/CIO film is shown in Figure 6a confirming the existence of cupric oxide with a monoclinic structure. No sign of the formation of a crystalline CIO shell is observed. To have a direct evidence on the formation of the copper iron oxide phase upon iron modification of the CuO nanowires, Raman spectra for the pristine and Fe-modified CuO electrode were acquired (Figure 6b). Except for the exact wavenumbers of the different contributions, the spectrum for pristine CuO agrees with those found in the literature.[49,50] As observed, iron modification leads to a shift of the main bands toward higher wavenumbers. More importantly, a new band and a new shoulder appear at 212 and 293 cm^{-1}, which would correspond to the bands reported for $CuFe_2O_4$ at 215 and 295 cm^{-1}.[51,52] These results thus suggest that iron modification leads to the formation of a poorly crystallized shell of $CuFe_2O_4$.

Moreover, the XPS spectra for the Cu 2p is shown in Figure 6c. As observed, the XPS signal of Cu 2p is similar to that obtained for pristine CuO and attributed completely to Cu^{2+}. The Fe 3p XPS signal (Figure 6d) shows a weak signal at a binding energy of 56 eV that can be assigned to Fe^{3+} present at a relatively low concentration in the sample. The Fe 2p XPS region is obscured by a contribution from copper and it is thus not shown.

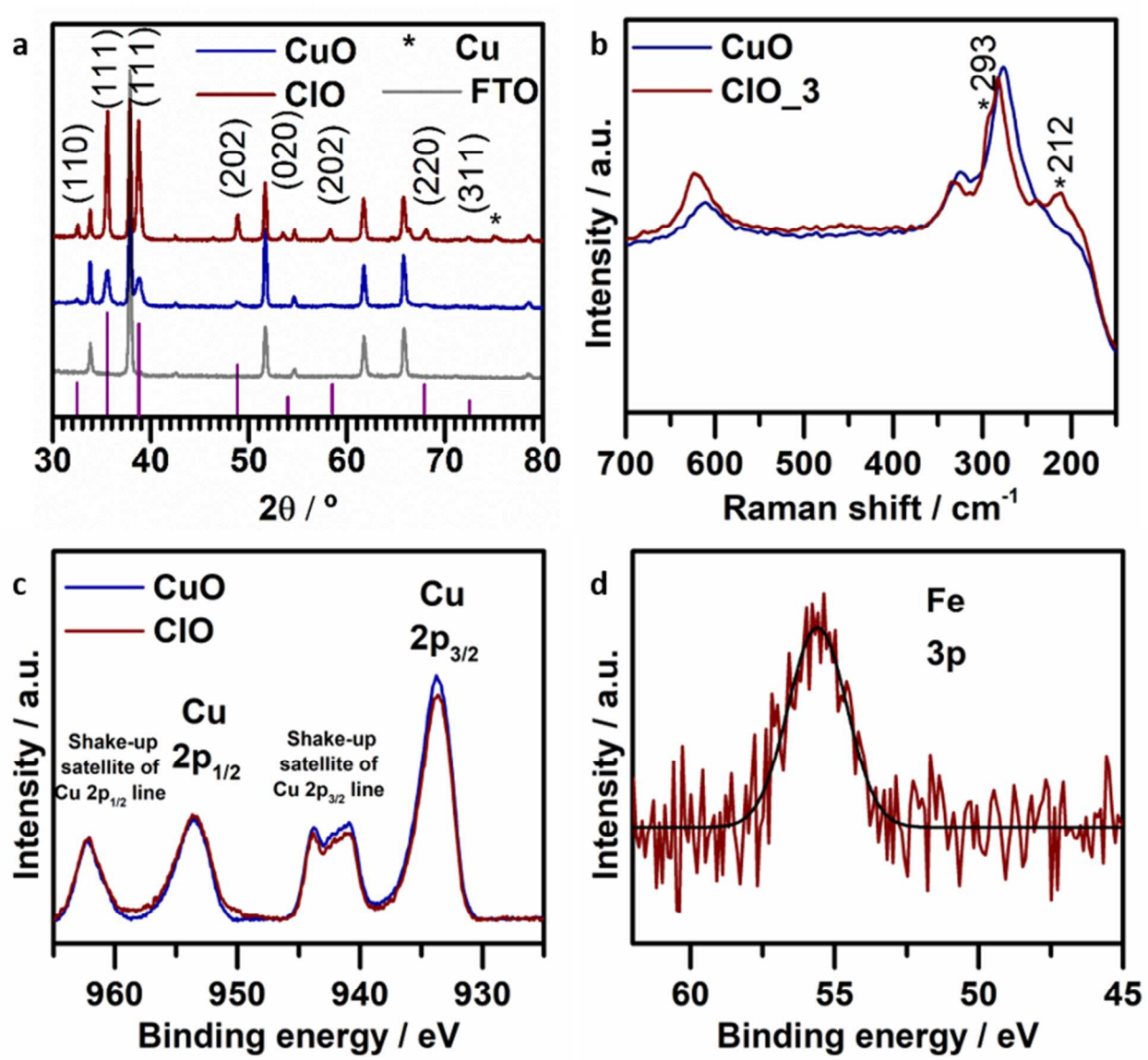

Figure 6. (a) X-ray diffractogram for pristine cupric oxide (blue) and CIO_3 (red). The cupric oxide main reflections are labeled. The unlabeled peaks correspond to the conducting glass substrate ($F:SnO_2$), (b) Raman spectra of pristine cupric oxide (blue) and CIO_3 (red), (c) Cu 2p XPS region for pristine copper oxide (II) (blue) and CIO_3 (red) and (d) Fe 2p XPS region for CIO_3.

(Photo)electrochemical characterization. The two variants of the impregnation procedure described in the experimental section have been studied. In turn, for the first procedure two types of additions have been assayed as describe above.

The CIO shell was observed to be more stable when the treatment was performed through casting *n* drops of a solution resulting from the dilution 1:*n* of the original one. Concretely, maximum stability was achieved when applying 4 droplets of a solution diluted by a factor of 4 (see Figure S4). This can be explained by considering that, in this way, the percolation of the iron precursor is better and thus the shell formation occurs throughout the entire length of the nanowire.

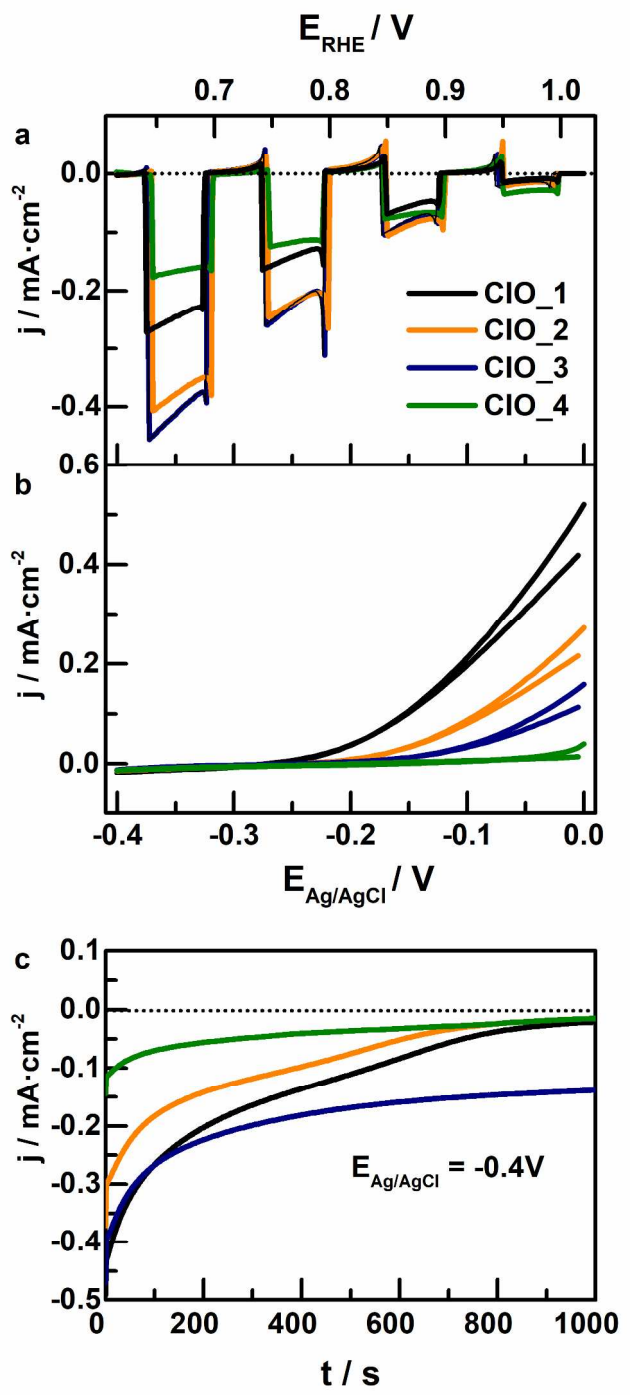

Figure 7. (Photo)electrochemical characterization in aqueous N_2-purged 1 M NaOH for the different cupric oxide modified with iron samples studied. (a) Linear voltammogram obtained under chopped illumination (320 mW·cm^{-2}, $\lambda > 350$ nm), (b) cyclic voltammogram obtained in the dark, and (c) chronoamperometry obtained under illumination (320 mW·cm^{-2}, $\lambda > 350$ nm) at a fixed potential of -0.4 V *vs.* Ag/AgCl.

The second variant of the preparation procedure consisted in changing the duration of the thermal treatment. The best (photo)response and stability were achieved when heating for 10 h instead of 5 h. Seemingly, a long thermal treatment promotes the phase transformation of surface CuO into CIO (see Figure S5).

Figure 7 shows the (photo)electrochemical characterization of the different CuO/CIO samples using the optimum conditions mentioned above (*i.e.* four drops of a 1:4 diluted precursor solution and 10 h of thermal treatment). In this case, the measurements were performed in the following order: *(i)* LSV under chopped illumination and *(ii)* cyclic voltammetry recorded in the dark in N_2-purged aqueous 1 M NaOH. Focusing on Figure 7a, upon iron modification, the photocurrents obtained in all cases are lower than those for pristine cupric oxide. It should be noted that the photocurrent initially increases upon the addition of iron, reaching an optimum value for CIO_3. Further increasing the iron loading leads to a substantial decrease of the (photo)currents. One could speculate that, for low loadings, the amount of iron is insufficient to form complete shells. Taking into account that $CuFe_2O_4$ is not a particularly good material for hydrogen evolution, it is easy to explain that, when amounts higher than that corresponding to CIO_3 were added, more $CuFe_2O_4$ was present in the surface of the photocathode and, therefore, less (photo)current was obtained. The voltammetric responses obtained in the dark (Figure 7b) after recording the photocurrents exhibit anodic currents probably coming from the re-oxidation of the products associated to the cathodic photocurrents as in the case of the pristine CuO electrode. Both hydrogen and reduced copper species (Cu(0) and Cu(I)) are expected to be the products associated to the cathodic photocurrents. The photogenerated hydrogen molecules quickly diffuse to the electrolyte bulk, while the reduced species of copper are expected to remain on the electrode surface, being available for re-oxidation upon the application of a high

enough potential. Importantly, the higher the loading of iron, the lower the anodic currents in the dark. These results clearly indicate that the protection with CIO drastically inhibits the photocorrosion of the CuO electrode.

Finally, Figure 7c shows the chronoamperometry obtained at -0.4 V *vs.* Ag/AgCl for 1000 s under continuous illumination (320 $mW \cdot cm^{-2}$, $\lambda > 350$ nm). The protective character of the $CuFe_2O_4$ deposit is clearly supported. It is worth noting that the best trade-off between (photo)current and stability was achieved for CIO_3, in which cupric oxide is covered by a shell of $CuFe_2O_4$ 8 nm in thickness. The relatively favorable band positions of CuO and copper ferrite shown in Scheme 1 support the extraction of the photogenerated electrons, allowing hydrogen evolution to proceed.

Scheme 1. Band alignment between CuO and $CuFe_2O_4$ in the core shell structure of the nanowires.

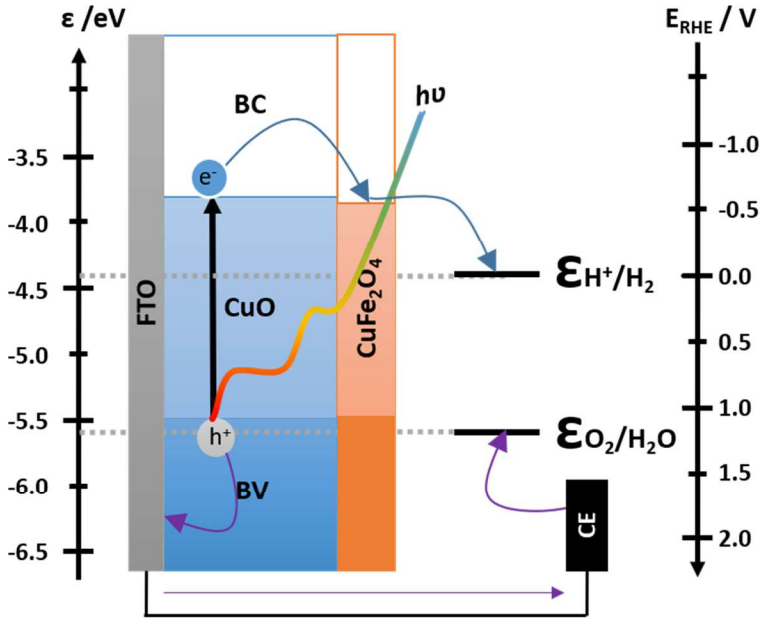

At this point, it seems useful to compare the behavior of a pristine CuO electrode with that of the optimum iron-modified electrode. This is done in Figure 8, which shows that iron modification

leads to a significant decrease of the photocurrent (Figure 8a), accompanied by a drastic decrease of the dark re-oxidation current (Figure 8b). Most importantly, iron modification also leads to a drastic enhancement of the photostability under intense illumination (Figure 8c).

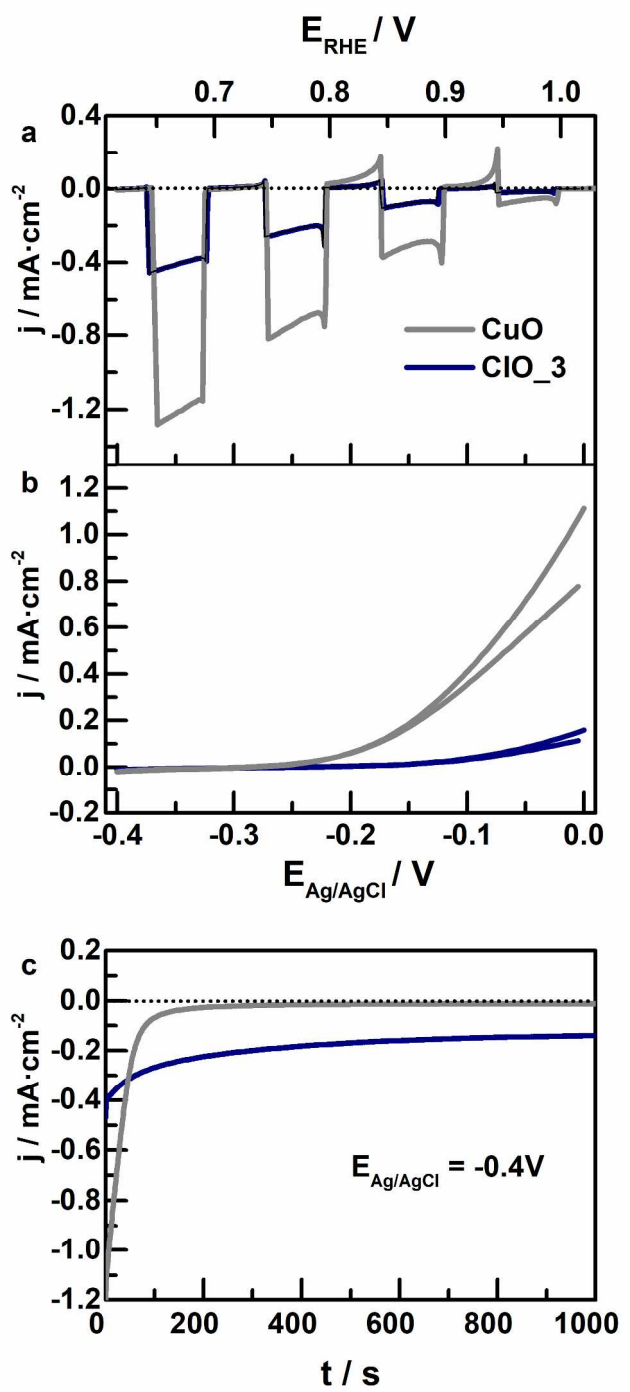

Figure 8. Comparison of the photoelectrochemical behavior of pristine cupric oxide and CIO_3 electrodes in aqueous N_2-purged 1 M NaOH; (a) Linear scan voltammograms obtained under chopped illumination (320 mW·cm^{-2}, λ > 350 nm), (b) cyclic voltammograms obtained in the dark, and (c) chronoamperometris curves obtained under illumination (320 mW·cm^{-2}, λ > 350 nm) at a potential of -0.4 V *vs.* Ag/AgCl.

In addition, EIS experiments were done under illumination (320 mW·cm^{-2}, λ > 350 nm) for CIO_3 electrodes (Figure 9) to assess the kinetics of charge transfer processes under PEC operating conditions. The same potentials as in the case of pristine cupric oxide were chosen: -0.1 V and -0.23 V *vs.* Ag/AgCl. Now the value of R_{sc} deduced from the spectra is much higher in agreement with the fact that both the CIO shell behaves as a barrier and the main electrochemical process changes from being mainly the reduction of CuO to being that of water, which is kinetically slower, giving rise to larger charge transfer resistances.

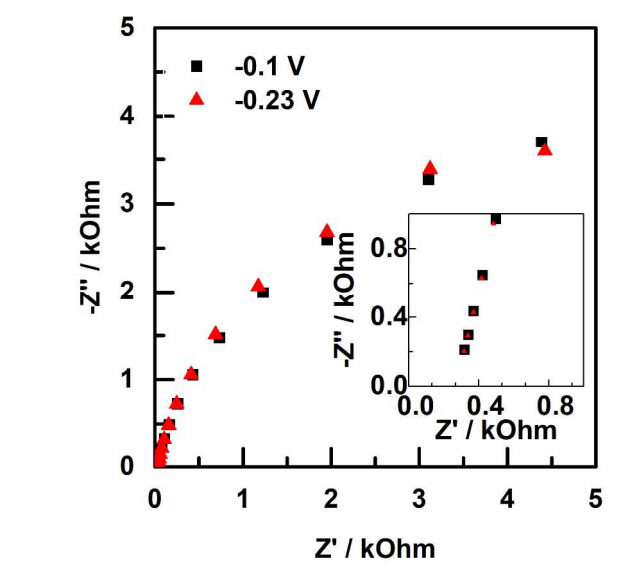

Figure 9. Nyquist plots for CIO_3 electrodes at -0.1 V *vs.* Ag/AgCl (square, black) and -0.23 V *vs.* Ag/AgCl (triangle, red) under illumination (320 mW·cm^{-2}, λ > 350 nm) in N_2-purged aqueous 1 M NaOH.

It is worth noting that the same methodology was employed to protect the CuO nanowires with magnesium. The employment of a magnesium precursor to protect CuO also leads to a

significant improvement in stability. However, a clear trend with the amount of uploaded Mg could not be discerned. The details of the procedure and the results obtained are shown at the Supporting Information.

Hydrogen gas measurements. Finally, hydrogen gas measurements were performed during 2800 s under continuous illumination at a constant applied current of 75 μA by means of gas chromatography (see Figure S6). Remarkably, for both pristine and iron-modified cupric oxide electrodes, the potential recorded during the chronopotentiometric experiment is roughly stable, particularly for the iron-modified electrode (Fig. S6). The amount of hydrogen corresponds to Faradaic efficiency values of 45% in the case of pristine cupric oxide and of about 100% for CIO_3 electrodes. These results confirm that, in the case of pristine cupric oxide, (photo)corrosion takes place, in addition to H_2 generation.

Discussion.

The FE-SEM images of the monoclinic cupric oxide electrodes do not reveal qualitative changes in morphology upon the addition of iron and its corresponding transformation into a ternary copper iron oxide ($CuFe_2O_4$, as suggested by Raman spectroscopy and XPS data indicating the prevalence of the oxidation states +2 and +3 for copper and iron, respectively). Importantly, the average diameter of the nanowires obtained upon modification with iron increases from 70 nm to 88 nm. These results roughly agree with the theoretical estimation of 8 nm of average thickness for the $CuFe_2O_4$ shell on the basis of the amount of Fe added. The XPS spectra of Cu *2p* reveal that the oxidation state of copper does not change upon the modification with iron, being +2 in both cases.

With respect to the Fe modification procedure, it has been clearly established that adding the same amount of precursor as *n* drops of a precursor solution diluted by a factor of 1:*n* yields electrode more efficient than applying only one drop of non-diluted precursor solution. Probably, by adding *n*-drops with the subsequent mild heating, the iron precursor solution can percolate more effectively the nanostructure and thus wet the entire surface of the nanowires from top to bottom, giving as a result better protection likely derived from the formation of a more homogeneous CIO shell. On the other hand, a sufficient duration of the thermal treatment is key to attain an effective protection, which is not unexpected as solid phase transformation is relatively slow due to diffusional limitations.

While the degree of protection against photocorrosion provided by the CIO layer is remarkable, admittedly the (photo)current also decreases. This is related to the fact that, prior to modification, CuO photocorrosion proceeds with a high Faradaic efficiency, while upon modification virtually all of the (photo)current leads to hydrogen evolution. Although the band edges probably straddle in an appropriate way the driving force for the transfer of electrons from the CuO to the CIO is not large. Finally, the fact that no co-catalyst is employed favors surface recombination. Probably, in the case of CuO, Cu(0) species can effectively act as co-catalysts for hydrogen evolution.

CONCLUSIONS

In this work, it has been shown that unprotected cupric oxide electrodes formed by nanowires prepared by copper electrodeposition and subsequent chemical oxidation + thermal treatment show a high photoactivity and a Faradaic efficiency for hydrogen evolution of around 45%, which means that the photocurrents are mainly derived from reductive photocorrosion. A

strategy based on surface phase transformation for stabilization against photocorrosion has been demonstrated to be effective. Specifically, the CuO nanowires constituting the thin film electrode are impregnated by an iron precursor and subjected to a thermal treatment that leads to the formation of a shell of a ternary copper iron oxide ($CuFe_2O_4$). In such a way a diffuse interfase is expected to form between core and shell, which should be beneficial to hinder interfacial recombination. Importantly, a significant stabilization of the CuO-based photocathodes together with a 100% Faradaic efficiency for hydrogen evolution has been demonstrated. Remarkably, an analogous strategy also showed to be effective when Mg is used for modification.

From a practical perspective, the methods reported here for electrode preparation and modification are cost-effective and have good scalability. The magnitude of the (photo)currents still requires improvement. Work is underway in our laboratory in several directions that include: ii) applying the method for CuO samples prepared through alternative routes and having different morphology ii) trying different metal modifiers as to tailor the composition and structure of the shell, and iii) adding co-catalysts to enhance the electron transfer, and thus, to increase the (photo)currents obtained.

ASSOCIATED CONTENT

Supporting Information. Additional experimental details, sample characterization, (photo)electrochemical characterization and a study of cupric oxide modified with magnesium are included in the Supporting Information.

AUTHOR INFORMATION

Corresponding Author

*E-mail: roberto.gomez@ua.es

ACKNOWLEDGMENT

Authors are grateful to MINECO of Spain for the financial support through project MAT2015-71727-R (FONDOS FEDER). A. C. wants to acknowledge the University of Alicante for a predoctoral grant (FPU-UA). Authors are also grateful to Dra. Teresa Lana-Villarreal for the acquisition of Raman spectra.

REFERENCES

(1) Gerosa, M.; Sacco, A.; Scalia, A.; Bella, F.; Chiodoni, A.; Quaglio M.; Tresso, M.; Bianco, S. Toward Totally Flexible Dye-Sensitized Solar Cells Based on Titanium Grids and Polymeric Electrolyte. *IIEE J. Photovoltaics* **2016**, *6,* 498-505.

(2) Bella, F.; Verna, A.; Gerbaldi, C. Patterning Dye-Sensitized Solar Cell Photoanodes through a Polymeric Approach: a Perspective. *Mater. Sci. Semicond. Process.* **2018**, *73*, 92-98.

(3) Gang, J.; Sumathy, K.; Qiao, Q.; Zhou, Z. Review on Dye-Sensitized Solar Cells (DSSCs): Advanced Techniques and Research Trends. *Renew. Sustain. Energy Rev.* **2017**, *68,* 234-246.

(4) Bella, F.; Muñoz-Garcia, A.B.; Meligrana, G.; Lamberti, A.; Destro, M.; Pavone, M.; Gerbaldi, C. Unveiling the Controversial Mechanism of Reversible Na Storage in TiO_2 Nanotubes Arrays: Amorphous versus Anatase TiO_2. *Nano Research.* **2017**, *10,* 2891-2903.

(5) Hwang, J.Y.; Myung, S.T.; Sun, Y.K. Sodium-Ion Batteries: Present and Future. *Chem. Soc. Rev.* **2017**, *46,* 3529-3614.

(6) Purkait, T.; Singh, G.; Kumar, D.; Mandeep, S.; Dey, R.S. High-Performance Flexible Supercapacitors Based on Electrochemically Tailored Three-Dimensional Reduced Graphene Oxide Networks. *Sci. Rep.* **2018**, *8,* 640-653.

(7) Jiang, C.; Moniz, S.J.A.; Wang, A.; Zhang, T.; Tang, J. Photoelectrochemical Devices for Solar Water Splitting- Materials and Challenges. *Chem. Soc. Rev.* **2017**, *46*, 4645-4660.

(8) Gray, H. B. Powering the Planet with Solar Fuel. *Nat. Chem.* **2009**, *1* , 7.

(9) Fujishima, A.; Honda, K. Electrochemical Photolysis of Water at a Semiconducr Electrode. *Nature* **1972**, *238*, 37–38.

(10) Walter, M. G.; Warren, E. L.; McKone, J. R.; Boettcher, S. W.; Mi, Q.; Santori, E. A.; Lewis, N. S. Solar Water Splitting Cells. *Chem. Rev.* **2010**, *110*, 6446–6473.

(11) Boettcher, S. W.; Warren, E. L.; Putnam, M. C.; Santori, E. A.; Turner-Evans, D.; Kelzenberg, M. D.; Walter, M. G.; McKone, J. R.; Brunschwig, B. S.; Atwater, H. A.; Lewis, N. S. Photoelectrochemical Hydrogen Evolution Using Si Microwire Arrays. *J. Am. Chem. Soc.* **2011**, *133*, 1216–1219.

(12) Niu, W.; Zhu, L.; Wang, Y.; Lou, Z.; Ye, Z. The Interfacial Study on the Cu_2O/Ga_2O_3 /AZO/TiO_2 Photocathode for Water Splitting Fabricated by Pulsed Laser Deposition. *Catal. Sci. Technol.* **2017**, *7*, 1602-1610.

(13) Wang, G.; Ling, Y.; Wang, H.; Xihong, L.; Li, Y. Chemically Modified Nanostructures for Photoelectrochemical Water Splitting. *J. Photochem. Photobiol. C Photochem. Rev.* **2014**, *18*, 35–51.

(14) Bak, T.; Nowotny, J.; Rekas, M.; Sorrell, C. Photo-Electrochemical Hydrogen Generation

from Water Using Solar Energy. Materials-Related Aspects. *Int. J. Hydrogen Energy* **2002**, *27*, 991–1022.

(15) Bornoz, P.; Abdi, F. F.; Tilley, S. D.; Dam, B.; Van De Krol, R.; Grätzel, M.; Sivula, K. A Bismuth Vanadate-Cuprous Oxide Tandem Cell for Overall Solar Water Splitting. *J. Phys. Chem. C* **2014**, *118*, 16959–16966.

(16) Prévot, M. S.; Sivula, K. Photoelectrochemical Tandem Cells for Solar Water Splitting. *J. Phys. Chem. C* **2013**, *117*, 17879–17893.

(17) Yu, Q.; Meng, X.; Wang, T.; Li, P.; Liu, L.; Chang, K.; Liu, G.; Ye, J. A Highly Durable P-$LaFeO_3$/n-Fe_2O_3 Photocell for Effective Water Splitting under Visible Light. *Chem. Commun.* **2015**, *51*, 3630–3633.

(18) Kim, J. H.; Kaneko, H.; Minegishi, T.; Kubota, J.; Domen, K. Overall Photoelectrochemical Water Splitting Using Tandem Cell under Simulated Sunlight. *ChemSusChem* **2016**, *9*, 61–66.

(19) Jian, J.; Jiang, G.; van de Krol, R.; Wei, B.; Wang, H. Recent Advances in Rational Engineering of Multinary Semiconductors for Photoelectrochemical Hydrogen Generation. *Nano Energy* **2018**, *51*, 457-480.

(20) Bolton, J. R.; Strickler, S. J.; Connolly, J. S. Limiting and Realizable Efficiencies of Solar Photolysis of Water. *Nature* **1985**, *316*, 495–500.

(21) Weber, M. F.; Dignam, M. J. Efficiency of Splitting Water with Semiconducting Photoelectrodes. *J. Electrochem. Soc.* **1984**, *131*, 1258-1265.

(22) Marschall, R. Semiconductor Composites: Strategies for Enhancing Charge Carrier Separation to Improve Photocatalytic Activity. *Adv. Funct. Mater.* **2014**, *24*, 2421–2440.

(23) Huang, Q.; Ye, Z.; Xiao, X. Recent Progress in Photocathodes for Hydrogen Evolution. *J. Mater. Chem. A* **2015**, *3*, 15824–15837.

(24) Tang, H.; Matin, M. A.; Wang, H.; Sudhakar, S.; Chen, L. E.; Al-jassim, M. M.; Yan, Y. Enhancing the Stability of CuO Thin-Film Photoelectrodes by Ti Alloying. *J. Electron. Mater.* **2012**, *41*, 3062–3067.

(25) Guo, X.; Diao, P.; Xu, D.; Huang, S.; Yang, Y.; Jin, T. CuO/Pd Composite Photocathodes for Photoelectrochemical Hydrogen Evolution Reaction. *Int. J. Hydrogen Energy* **2014**, *9*, 2–12.

(26) Masudy-Panah, S.; Siavash Moakhar, R.; Chua, C. S.; Kushwaha, A.; Dalapati, G. K. Stable and Efficient CuO Based Photocathode through Oxygen-Rich Composition and Au-Pd Nanostructure Incorporation for Solar-Hydrogen Production. *ACS Appl. Mater. Interfaces* **2017**, *9*, 27596–27606.

(27) Septina, W.; Prabhakar, R. R.; Wick, R.; Moehl, T.; Tilley, S. D. Stabilized Solar Hydrogen Production with CuO/CdS Heterojunction Thin Film Photocathodes. *Chem. Mater.* **2017**, *29*, 1735–1743.

(28) Nakaoka, K.; Ueyama, J.; Ogura, K. Photoelectrochemical Behavior of Electrodeposited CuO and Cu_2O Thin Films on Conducting Substrates. *J. Electrochem. Soc.* **2004**, *115,* 661–665.

(29) Zheng, J. Y.; Song, G.; Kim, C. W.; Kang, Y. S. Facile Preparation of P-CuO and P-CuO/n-$CuWO_4$ Junction Thin Films and Their Photoelectrochemical Properties. *Electrochim. Acta* **2012**, *69*, 340–344.

(30) Luo, J.; Steier, L.; Son, M. K.; Schreier, M.; Mayer, M. T.; Grätzel, M. Cu_2O Nanowire Photocathodes for Efficient and Durable Solar Water Splitting. *Nano Lett.* **2016**, *16*, 1848–1857.

(31) Bai, Z.; Zhang, Y. A Cu_2O/Cu_2S-ZnO/CdS Tandem Photoelectrochemical Cell for Self-Driven Solar Water Splitting. *J. Alloys Compd.* **2017**, *698*, 133–140.

(32) Siol, S.; Hellmann, J. C.; Tilley, S. D.; Graetzel, M.; Morasch, J.; Deuermeier, J.; Jaegermann, W.; Klein, A. Band Alignment Engineering at Cu_2O/ZnO Heterointerfaces. *ACS Appl. Mater. Interfaces* **2016**, *8*, 21824–21831.

(33) Niu, W.; Moehl, T.; Cui, W.; Wick-Joliat, R.; Zhu, L.; Tilley, S. D. Extended Light Harvesting with Dual Cu_2O-Based Photocathodes for High Efficiency Water Splitting. *Adv. Energy Mater.* **2018,** *8,* 1702323.

(34) Azevedo, J.; Tilley, S. D.; Schreier, M.; Stefik, M.; Sousa, C.; Araújo, J. P.; Mendes, A.; Grätzel, M.; Mayer, M. T. Tin Oxide as Stable Protective Layer for Composite Cuprous Oxide Water-Splitting Photocathodes. *Nano Energy* **2016**, *24*, 10–16.

(35) Lee, Y. S.; Chua, D.; Brandt, R. E.; Siah, S. C.; Li, J. V.; Mailoa, J. P.; Lee, S. W.; Gordon, R. G.; Buonassisi, T. Atomic Layer Deposited Gallium Oxide Buffer Layer Enables 1.2 V Open-Circuit Voltage in Cuprous Oxide Solar Cells. *Adv. Mater.* **2014**, *26*, 4704–4710.

(36) Ida, S.; Yamada, K.; Matsunaga, T.; Hagiwara, H.; Matsumoto, Y.; Ishihara, T. Preparation of p-Type $CaFe_2O_4$ Photocathodes for Producing Hydrogen from Water. *J. Am. Chem. Soc.* **2010**, *132*, 17343–17345.

(37) Matsumoto, Y.; Omae, M.; Sugiyama, K.; Sato, E. New Photocathode Materlals for Hydrogen Evolution: $CaFe_2O_4$ and $Sr_7Fe_{10}O_{22}$. *J. Phys. Chem.* **1987**, *91*, 577–581.

(38) Díez-García, M. I.; Gómez, R. Investigating Water Splitting with $CaFe_2O_4$ Photocathodes by Electrochemical Impedance Spectroscopy. *ACS Appl. Mater. Interfaces* **2016**, *8*, 21387–21397.

(39) Joshi, U. A.; Maggard, P. A. $CuNb_3O_8$: A p-Type Semiconducting Metal Oxide Photoelectrode. *J. Phys. Chem. Lett.* **2012**, *3*, 1577–1581.

(40) Prévot, M. S.; Guijarro, N.; Sivula, K. Enhancing the Performance of a Robust Sol-Gel-Processed p-Type Delafossite $CuFeO_2$ Photocathode for Solar Water Reduction. *ChemSusChem* **2015**, *8*, 1359–1367.

(41) Díaz-García, A. K.; Lana-Villarreal, T.; Gómez, R. Sol–gel Copper Chromium Delafossite Thin Films as Stable Oxide Photocathodes for Water Splitting. *J. Mater. Chem. A* **2015**, *3*, 19683–19687.

(42) Díez-García, M. I.; Gómez, R. Metal Doping to Enhance the Photoelectrochemical Behavior of $LaFeO_3$ Photocathodes. *ChemSusChem* **2017**, *10*, 2457–2463.

(43) Masudy-Panah, S.; Siavash Moakhar, R.; Chua, C. S.; Tan, H. R.; Wong, T. I.; Chi, D.; Dalapati, G. K. Nanocrystal Engineering of Sputter-Grown CuO Photocathode for

Visible-Light-Driven Electrochemical Water Splitting. *ACS Appl. Mater. Interfaces* **2016**, *8*, 1206–1213.

(44) Lee, J. G.; Kim, D.-Y.; Lee, J.-H.; Kim, M.; An, S.; Jo, H. S.; Nervi, C.; Al-Deyab, S. S.; Swihart, M. T.; Yoon, S. S. Scalable Binder-Free Supersonic Cold Spraying of Nanotextured Cupric Oxide (CuO) Films as Efficient Photocathodes. *ACS Appl. Mater. Interfaces* **2016**, *8*, 15406–15414.

(45) Jamali, S.; Moshaii, A. Improving Photo-Stability and Charge Transport Properties of Cu_2O/CuO for Photo-Electrochemical Water Splitting Using Alternate Layers of WO_3 or $CuWO_4$ Produced by the Same Route. *Appl. Surf. Sci.* **2017**, *419*, 269–276.

(46) Hsu, Y.; Yu, C.; Lin, H.; Chen, Y.; Lin, Y. Template Synthesis of Copper Oxide Nanowires for Photoelectrochemical Hydrogen Generation. *J. Electroanal. Chem.* **2013**, *704*, 19–23.

(47) Tahir, D.; Tougaard, S. Electronic and Optical Properties of Cu, CuO and Cu_2O Studied by Electron Spectroscopy. *J. Phys. Condens. Matter* **2012**, *24*, 175002.

(48) Dubale, A. A.; Pan, C.-J.; Tamirat, A. G.; Chen, H.-M.; Su, W.-N.; Chen, C.-H.; Rick, J.; Ayele, D. W.; Aragaw, B. A.; Lee, J.-F.; Yang, Y.-W.; Hwang, B.-J. Heterostructured Cu_2O/CuO Decorated with Nickel as a Highly Efficient Photocathode for Photoelectrochemical Water Reduction. *J. Mater. Chem. A* **2015**, *3*, 12482–12499.

(49) Debbichi, L.; Marco de Lucas, M. C.; Pierson, J. F.; Krüger, P. Vibrational Properties of CuO and Cu_4O_3 from First-Principles Calculations, and Raman and Infrared Spectroscopy. *J. Phys. Chem. C* **2012**, *116*, 10232–10237.

(50) Deng, Y.; Handoko, A. D.; Du, Y.; Xi, S.; Yeo, B. S. *In Situ* Raman Spectroscopy of Copper and Copper Oxide Surfaces during Electrochemical Oxygen Evolution Reaction: Identification of Cu^{III} Oxides as Catalytically Active Species. *ACS Catal.* **2016**, *6*, 2473–2481.

(51) Balaji, M.; Chithra Lekha, P.; Pathinettam Padiyan, D. Core-Shell Structure in Copper Ferrite-Polyaniline Nanocomposite: Confirmation by Laser Raman Spectra. *Vib. Spectrosc.* **2012**, *62*, 92–97.

(52) Chatterjee, B. K.; Bhattacharjee, K.; Dey, A.; Ghosh, C. K.; Chattopadhyay, K. K. Influence of Spherical Assembly of Copper Ferrite Nanoparticles on Magnetic Properties: Orientation of Magnetic Easy Axis. *Dalt. Trans.* **2014**, *43*, 7930–7944.

TABLE OF CONTENTS (TOC)